Rational Synthesis and Structural Characterizations of Complex $TiSi_2$ Nanostructures

Sa Zhou, Xiaohua Liu, Yongjing Lin, and Dunwei Wang*

Department of Chemistry, Merkert Chemistry Center, Boston College, 2609 Beacon Street, Chestnut Hill, Massachusetts 02467

Received August 29, 2008. Revised Manuscript Received January 12, 2009

We present in this article our successes in synthesizing $TiSi_2$ nanostructures with various complexities using a chemical vapor deposition (CVD) method. Attention has been paid to understanding the growth mechanism. The governing factor was found to be the surface energy differences between various crystal planes of orthorhombic $TiSi_2$ (C54 and C49), because of their specific atomic arrangements of Si and Ti on the surfaces. This understanding has allowed us to control the growth morphologies and obtained one-dimensional (1D) nanowires, two-dimensional (2D) nanonets and three-dimensional (3D) complexes with rational designs by tuning the precursor chemical reactions. Careful studies of the atomically-resolved microstructures revealed the existence of distorted C54 phases in 3D complexes, which was attributed to playing the key role in the unique structure formation. These results are expected to shed light on metal silicide nanostructure growths broadly and to present opportunities for novel nanostructure syntheses.

Nanoscale metal silicides can serve as low-resistance contacting and/or interconnecting materials in next generation's electronics, optoelectronics, and energy conversion devices. Much attention has been attracted to chemically synthesized various silicide nanowires (NWs), including iron silicide,[1] nickel silicide,[2] cobalt silicide,[3] chromium silicide,[4] tantalum silicide,[5] titanium silicide,[6,7] and ternary silicides.[8] Because these silicides can assume various stoichiometry and/or crystal structures, the detailed growth mechanisms largely remain illusive. New phenomena differing from commonly observed NW growth mechanisms such as vapor−liquid−solid (VLS) have been reported. The understanding of the emerging silicide growths is expected to provide information that will enrich our knowledge of the synthetic processes on the nanoscale; it is also anticipated to present opportunities to control the synthesis and thus to create new structures that are significant to a variety of interesting applications.

For one example, the promises that nanoscale materials hold in electronics[9] or high-efficiency energy applications[10] by and large stem from their unique dimensions — most charge-related processes (e.g., charge separation, transport and recombination) occur on the relevant length scale of nanometers. It is therefore desirable to pursue materials that offer superior charge transport pathways similar to that in a bulk crystal. Yet, the materials should also share the advantages characteristic to nanomaterials such as small dimensions in its fine structures (particularly important to nanoelectronics) or high surface areas (a desired asset for energy conversions). Within the context, two- or three-dimensional complex nanostructures are appealing candidates.[11] Recently, we successfully synthesized two-dimensional (2D) nanonets (NNs) of $TiSi_2$.[7] The distinction of our approach lies in that no heterogeneous growth seeds were involved. Thus, it eliminates the necessity of introducing impurities to initiate the growth. In this article, we further the discussions of our understandings of the detailed growth mechanisms. The understanding in turn has allowed us to

* Corresponding author. E-mail: dunwei.wang@bc.edu. Tel: (617) 552-3121. Fax: (617) 552-2705.

(1) Varadwaj, K. S. K.; Seo, K.; In, J.; Mohanty, P.; Park, J.; Kim, B. *J. Am. Chem. Soc.* **2007**, *129*, 8594–8599.
(2) (a) Decker, C. A.; Solanki, R.; Freeouf, J. L.; Carruthers, J. R.; Evans, D. R. *Appl. Phys. Lett.* **2004**, *84*, 1389–1391. (b) Song, Y. P.; Schmitt, A. L.; Jin, S. *Nano Lett.* **2007**, *7*, 965–969. (c) Zhang, H. L.; Li, F.; Liu, C.; Cheng, H. M. *Nanotechnology* **2008**, *19*.
(3) Schmitt, A. L.; Zhu, L.; Schmeisser, D.; Himpsel, F. J.; Jin, S. *J. Phys. Chem. B* **2006**, *110*, 18142–18146.
(4) Szczech, J. R.; Schmitt, A. L.; Bierman, M. J.; Jin, S. *Chem. Mater.* **2007**, *19*, 3238–3243.
(5) Chueh, Y. L.; Ko, M. T.; Chou, L. J.; Chen, L. J.; Wu, C. S.; Chen, C. D. *Nano Lett.* **2006**, *6*, 1637–1644.
(6) (a) Lin, H.-K. Tzeng, Y.-F. Wang, C.-H. Tai, N.-H. Lin, I. N. Lee, C.-Y. Chiu, H.-T. *Chem. Mater.* **2008**, *20*, 2429–2431. (b) Xiang, B. Wang, Q. X. Wang, Z. Zhang, X. Z. Liu, L. Q. Xu, J. Yu, D. P. *Appl. Phys. Lett.* **2005**, *86,* 243103/1-3.
(7) Zhou, S.; Liu, X. H.; Lin, Y. J.; Wang, D. W. *Angew. Chem., Int. Ed.* **2008**, *47*, 7681–7684.
(8) Schmitt, A. L.; Higgins, J. M.; Jin, S. *Nano Lett.* **2008**, *8*, 810–815.
(9) (a) Lieber, C. M. *Mater. Res. Bull.* **2003**, *28*, 486–491. (b) Xia, Y. N.; Yang, P. D.; Sun, Y. G.; Wu, Y. Y.; Mayers, B.; Gates, B.; Yin, Y. D.; Kim, F.; Yan, Y. Q. *Adv. Mater.* **2003**, *15*, 353–389.
(10) (a) Hochbaum, A. I.; Chen, R.; Delgado, R. D.; Liang, W.; Garnett, E. C.; Najarian, M.; Majumdar, A.; Yang, P. *Nature* **2008**, *451*, 163–167. (b) Garnett, E. C.; Yang, P. *J. Am. Chem. Soc.* **2008**, *130*, 9224–9225. (c) Boukai, A. I.; Bunimovich, Y.; Tahir-Kheli, J.; Yu, J.-K.; Goddard Iii, W. A.; Heath, J. R. *Nature* **2008**, *451*, 168–171. (d) Tian, B.; Zheng, X.; Kempa, T. J.; Fang, Y.; Yu, N.; Yu, G.; Huang, J.; Lieber, C. M. *Nature* **2007**, *449*, 885–889. (e) Maiolo, J. R.; Kayes, B. M.; Filler, M. A.; Putnam, M. C.; Kelzenberg, M. D.; Atwater, H. A.; Lewis, N. S. *J. Am. Chem. Soc.* **2007**, *129*, 12346–12347. (f) Goodey, A. P.; Eichfeld, S. M.; Lew, K. K.; Redwing, J. M.; Mallouk, T. E. *J. Am. Chem. Soc.* **2007**, *129*, 12344–12345.
(11) (a) Gur, I.; Fromer, N. A.; Chen, C. P.; Kanaras, A. G.; Alivisatos, A. P. *Nano Lett.* **2007**, *7*, 409–414. (b) Manna, L.; Milliron, D. J.; Meisel, A.; Scher, E. C.; Alivisatos, A. P. *Nat. Mater.* **2003**, *2*, 382–385. (c) Wang, D.; Qian, F.; Yang, C.; Zhong, Z. H.; Lieber, C. M. *Nano Lett.* **2004**, *4*, 871–874. (d) Wang, D. L.; Lieber, C. M. *Nat. Mater.* **2003**, *2*, 355–356.

10.1021/cm8023296 CCC: $40.75
Published on Web 02/11/2009

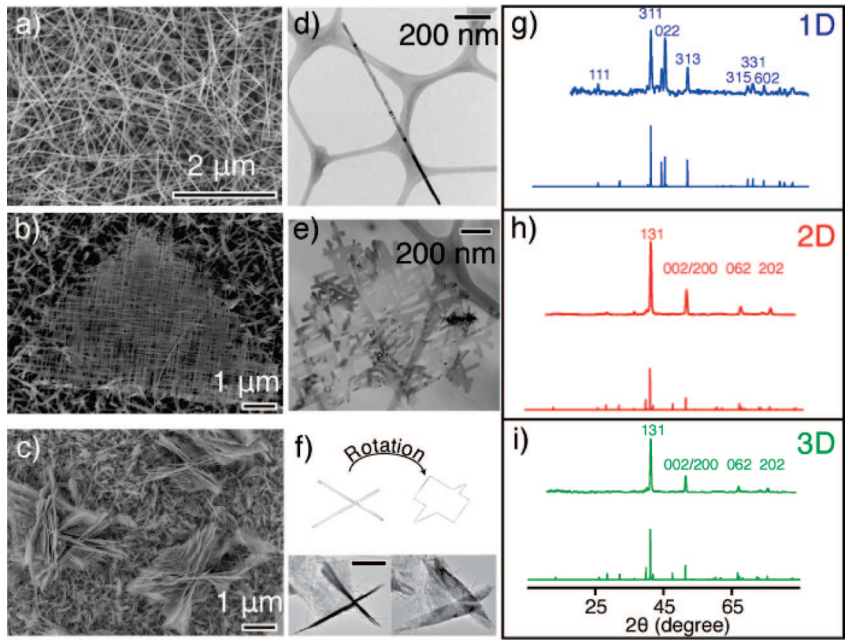

Figure 1. Morphologies and structures of various $TiSi_2$ nanostructures. (a, d, g) 1D NWs (C54 $TiSi_2$); (b, e, h) 2D NNs (C49 $TiSi_2$); (c, f, i) 3D complexes (C49 $TiSi_2$). Scale bar in f: 1 μm.

systematically vary the reaction conditions and to produce $TiSi_2$ nanostructures ranging from one-dimensional (1D) NWs to three-dimensional (3D) complexes.

Experimental Section

Synthesis. $TiSi_2$ nanostructures were synthesized in a home-built chemical vapor deposition (CVD) apparatus with SiH_4 (10% diluted in He, Airgas) and $TiCl_4$ (Sigma-Aldrich) as the precursors. The liquid $TiCl_4$ was contained in a stainless steel cylinder that was kept at room temperature and released through a metered controlling valve. It was carried into the growth chamber by a H_2-gas flow (100 standard cubic centimeters per minute, or sccm). 50 sccm SiH_4 was introduced to the chamber in tandem. The pressure was automatically controlled (2−7 Torr) through a throttle valve coupled with a pressure transducer. Typical growths were performed at T = 625−700 °C. The products were collected on a bare Si substrate that was cleaned following the standard clean room procedures, i.e., sonications in acetone, methanol, and isopropanol (see the Supporting Information for details).

Characterization. A scanning electron microscope (SEM, JEOL 6340F), a transmission electron microscope (TEM, JEOL 2010F), a X-ray diffractrometer (XRD, Bruker) and a X-ray photoelectron spectrometer (Kratos AXIS Ultra Imaging) were utilized for structural characterizations. Atomic structure and XRD pattern simulations were conducted with the Modeling software Materials Studio (MS) (Version 3.0.1, Accelrys).

Results and Discussion

Figure 1 summarizes various $TiSi_2$ nanostructures obtained in our studies. Scanning electron micrographs (SEM, a−c) and transmission electron micrographs (TEM, d−f) confirmed the 1D to 3D morphologies. X-ray diffraction patterns (XRD, g-i) and electron diffraction patterns (ED, not shown here) revealed the crystal structures. 1D NWs are composed of C54 while 2D NNs and 3D complexes are C49 $TiSi_2$. Lattice constants were calculated from the XRD patterns (a = 8.237 Å, b = 4.782 Å, c = 8.505 Å for C54 and a = 3.564 Å, b = 13.334 Å, c = 3.547 Å for C49, see Table S1 in the Supporting Information for tabulated comparison with literature), in excellent agreement with the literature values.[12] For all observed morphologies, the overall size of any complete structure, i.e., the length of a NW, the span of a NN, or the side of a 3D complex, is ∼2−10 μm, and the width of its components, i.e., the diameter of a NW and the

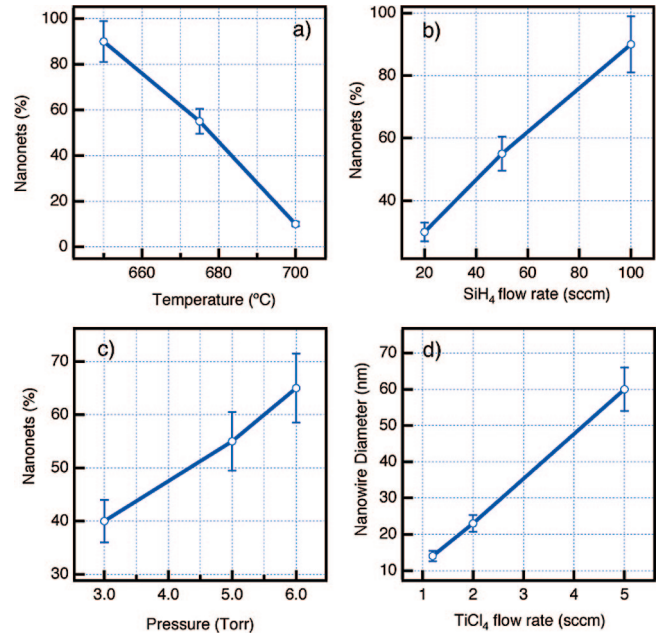

Figure 2. Influence of growth parameters on the products. (a−c) percentage of NNs as a function of temperature (a), SiH_4 feeding (b), and pressure (c). (d) Nanowire diameters increase as $TiCl_4$ feeding is increased. The percentage of the products was estimated by counting the volume occupations of different morphologies. The error bars represent standard deviations of the measurements on various samples. Each data point was calculated on the basis of measurements done on typically more than 10 samples.

(12) Beyers, R.; Sinclair, R. *J. Appl. Phys.* **1985**, *57*, 5240–5245.

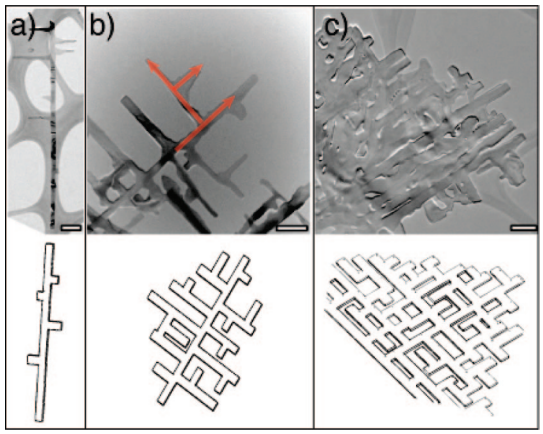

Figure 3. Evolution of a 2D $TiSi_2$ NN. Scale bars: 100 nm.

Table 1. Elemental Analysis of $TiSi_2$ Nanostructures

methods	Si	Ti	Si:Ti
EDS (C54 TiSi2)	0.667	0.333	2:1
EDS (C49 TiSi2)	0.714	0.286	5:2
XPS (C49 TiSi2)[a]	0.366	0.046	8:1

[a] O and Cl amount to 59% on the surface because of oxidations.

composing beams of a 2D NN or a 3D complex, is between 20−100 nm, highlighting the typical high anisotropy of the products (length/diameter: ∼20−500).

A highly anisotropic growth often involves processes that can drastically alter surface energies during the synthesis. To create 1D NWs, for example, one may introduce liquid droplets to significantly reduce the energy of atomic additions in one direction while maintaining the others unchanged as in the VLS mechanism. Conversely, surface passivations can be applied to increase the energy of additions in all directions but one, thus to limit the growth to the unpassivated direction. Because no growth seeds were observed in our $TiSi_2$ nanostructure synthesis (see Figure S1 in the Supporting Information), it is reasonable to conjecture that the growth proceeds following a vapor−solid (VS) mechanism. The surface energy differences among various crystal planes are the key to the unique morphologies. Careful examinations of the atomic arrangement of $TiSi_2$ showed that C49 $TiSi_2$ consists of a layer of Si atoms (the Si-terminated {010} plane; see Figure S3 in the Supporting Information).[13] Such layers are absent in C54 $TiSi_2$. We propose that the difference in detailed atomic arrangements acts as the defining factor. That is, because of the existence of the Si layer in C49, $TiSi_2$ preferably grows into C49 when the concentration of Si species is high. Next, we show experimental evidence to support this hypothesis.

We first sought to vary parameters important to the CVD synthesis, including pressure, temperature, precursor composition, and feeding rate. To keep the discussions concise, we only present parameters under which high yield $TiSi_2$ nanostructures were successfully produced. As recapitulated in Figure 2, C54 NWs and 49 NNs cogrew and their relative yield changed depending on the varying parameters. Higher pressures, lower temperatures, more SiH_4 and less $TiCl_4$ feeding favored C49 NNs. These conditions also favor higher Si:Ti ratios in the growth chamber. The key reactions that are involved in the synthesis are

$$TiCl_4 + 2H_2 \rightarrow Ti + 4HCl \quad (1)$$

$$SiH_4 \rightarrow Si + 2H_2 \quad (2)$$

The pyrolysis of SiH_4 is expected to be more sensitive to pressure than that of $TiCl_4$;[14] conversely, temperature has a relatively more profound influence on $TiCl_4$ decomposition than on SiH_4.[15] In the low pressure range, Si feeding from SiH_4 decomposition increases as the pressure is increased. Thus, lower temperatures and higher pressures produce a higher concentration of Si species. The higher yield of NNs under these conditions indicates that the presence of more Si species favor C49 $TiSi_2$ growth. In addition, the fact that more NNs grew when the SiH_4 feeding was increased also fits well to the predictions of our hypothesis.

At relatively low Si:Ti ratios, C54 $TiSi_2$ grows and forms NWs. This may be explained by the energy differences among various crystal planes of C54 $TiSi_2$. As an approximate quasi-quantitative comparison, we conducted calculations of the density of broken bonds on various crystal faces of C54 $TiSi_2$. Our preliminary results (Table S2 in the Supporting Information) showed that further Ti and Si depositions on the {010} planes lead to ∼33% energy reduction as compared to the depositions on other planes. Similar conclusions were reached by Iannuzzi et al., too.[13] As a result, during the C54 $TiSi_2$ growth, additions of Ti and Si atoms preferably take the {010} planes, leading to NW morphologies. It should be noted that the 1D growth was susceptible to the parameter variations and primarily took place when the overall concentrations of Ti and Si were relatively low, within which range more Ti feeding tended to produce fatter NWs (Figure 2d). We also note that we ruled out the possibilities that 1D NWs were first grown into C49 and then later converted into C54. This conclusion was based on two observations. First, we observed no C49 NWs without branches, suggesting that the C49 NW to C54 NW conversion is highly unlikely. Second, our thermal annealing tests showed remarkable stabilities of C49 $TiSi_2$ nanostructures: the C49 phase was maintained after 900 °C annealing for half an hour. It further strengthens our argument that the C54 NWs were not converted from C49 ones. We emphasize the unusual thermal stabilities of C49 $TiSi_2$ that have not been observed in bulk materials.[12] The small dimensions, the Si capping of the {010} planes and the lack of stacking faults along the ⟨010⟩ directions may all contribute to this result, although more studies are needed to elucidate the details.

Taken as a whole, the existence of complete Si-terminations in the {010} planes renders them unfavorable for further Ti and Si depositions in C49 $TiSi_2$. Further additions of atoms primarily take place on other crystal planes. From the

(13) Iannuzzi, M.; Miglio, L. *Surf. Sci.* **2001**, *479*, 201–212.

(14) Zhao, H. Z.; Zhou, S.; Hasanali, Z.; Wang, D. W. *J. Phys. Chem. C* **2008**, *112*, 5695–5698.

(15) (a) Robertson, R.; Hils, D.; Gallagher, A. *Chem. Phys. Lett.* **1984**, *103*, 397–404. (b) Sherman, A. Thermal Cvd of Metallic Conductors. In *Chemical Vapor Deposition for Microelectronics*; William Andrew Inc.: Norwich, NY, 1987; p 92. (c) Bryant, W. A. *J. Mater. Sci.* **1977**, *12*, 1285–1306.

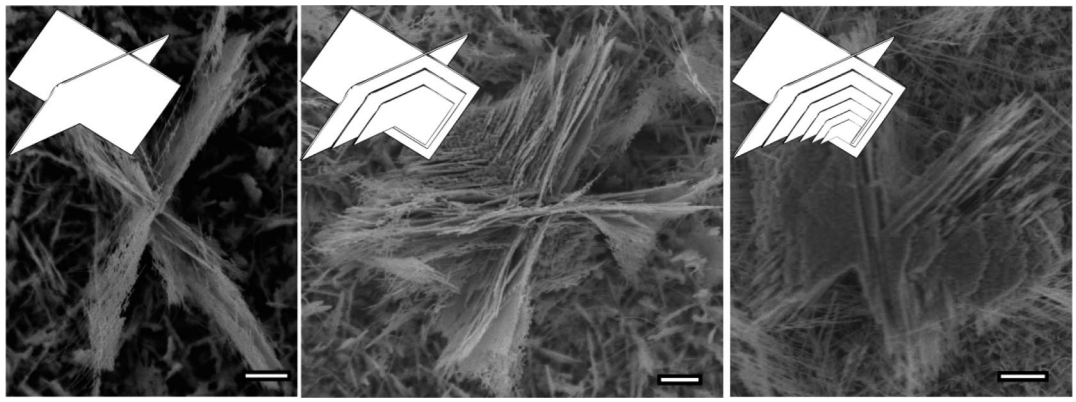

Figure 4. Growth of a 3D $TiSi_2$ nanostructure. Scale bars: 1 μm.

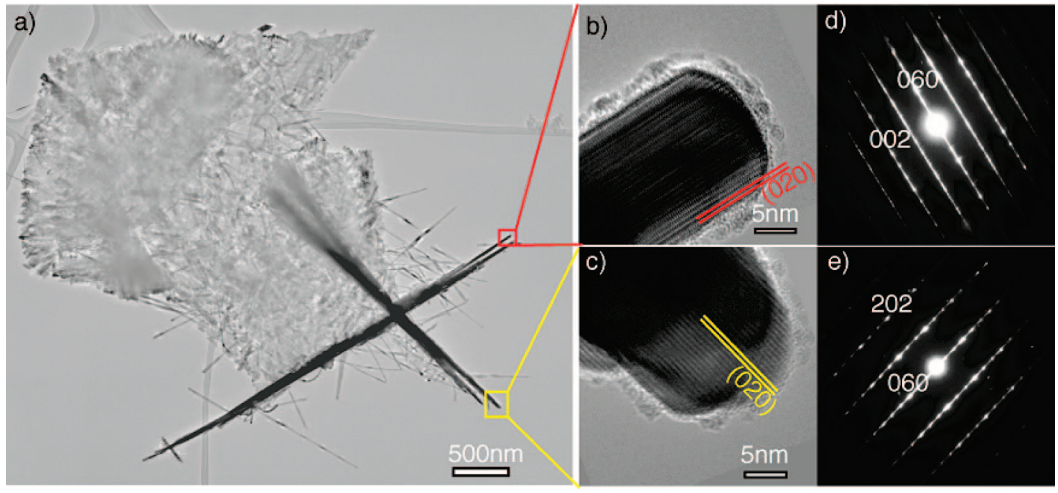

Figure 5. Microstructures of a 3D $TiSi_2$ complex. The overall structure is shown in a. High-magnification images (b, c) and corresponding ED patterns (d, e) show that the growth orientations are perpendicular to the *b* axis.

evolution of a 2D NN as shown in Figure 3, one can see that the growth exclusively takes place along the ⟨100⟩ and ⟨001⟩ directions, with nearly identical growth kinetics for either direction. The thickness of NNs rarely exceeded 20 nm. Si-terminations on the {010} planes were confirmed by elemental analyses using energy dispersive spectra (EDS) and X-ray photoelectron spectra (XPS) as summarized in Tab. 1. Si:Ti = 5:2 was derived from EDS although both ED and XRD patterns on the crystal structure analyses unambiguously confirmed that the material was indeed $TiSi_2$ (i.e., Ti:Si = 1:2). Further characterizations by XPS revealed that Si:Ti ratios on the surfaces (escape depth <1.5 nm) were even higher (∼8:1). The apparent discrepancy between structural and elemental characterizations can only be explained by the surface coverage of Si-atoms on the {010} planes.

In addition to 1D NWs and 2D NNs, we also obtained 3D $TiSi_2$ complexes (Figure 1c). Interestingly, they appeared as "X" shaped crosses with the flaps identified as 2D NNs (Figures 4 and 5). Within a given "X" cross, one group of flaps was always found to intercept with those from the other group at 120°. The characteristic is clearly manifested in Figure 4, which shows a series of SEM pictures of 3D $TiSi_2$ complexes at different stages of growths. Also shown here, when another layer of NN flaps were added to the existing 3D structure, they grew parallel to the existing ones. Both ED and XRD data confirmed that they are C49 structure $TiSi_2$ (Figure 1i and patterns d and e in Figure 5). The 3D complexes were observed under growth conditions where both NWs and NNs, i.e., C54 and C49 phases, coexisted. These conditions are typified by intermediate Si:Ti ratios: higher ones favor NNs, whereas lower ones favor NWs. It suggests a transitional character of the 3D complexes growths.

HRTEM was utilized to carefully examine the microstructures, and we discovered the existence of a distorted C54 phases, also denoted in the literature as C40.[16] As shown in Figure 6a, the C40 branches exist in the plane that is perpendicular to the NNs. They branch out at 120° (or 60°) angles relative to the NNs, suggesting a hexagonal symmetry. Indeed, with less than 3% lattice mismatch to the C54 phase, C40 $TiSi_2$ is characterized by the hexagonal symmetry, which is better shown in the diffraction pattern in Figure 6c. Confirmed by the HR imaging and ED are the [0001] zone axis of the C40 branches when viewed from the top. The {0001} planes are highly susceptible to further additions of Ti and Si atoms. Figure 6b shows the initial growth of C49 $TiSi_2$ on top of C40, whose ED pattern is shown in Figure

(16) Li, K.; Chen, S. Y.; Shen, Z. X. *Appl. Phys. Lett.* **2001**, *78*, 3989–3991.

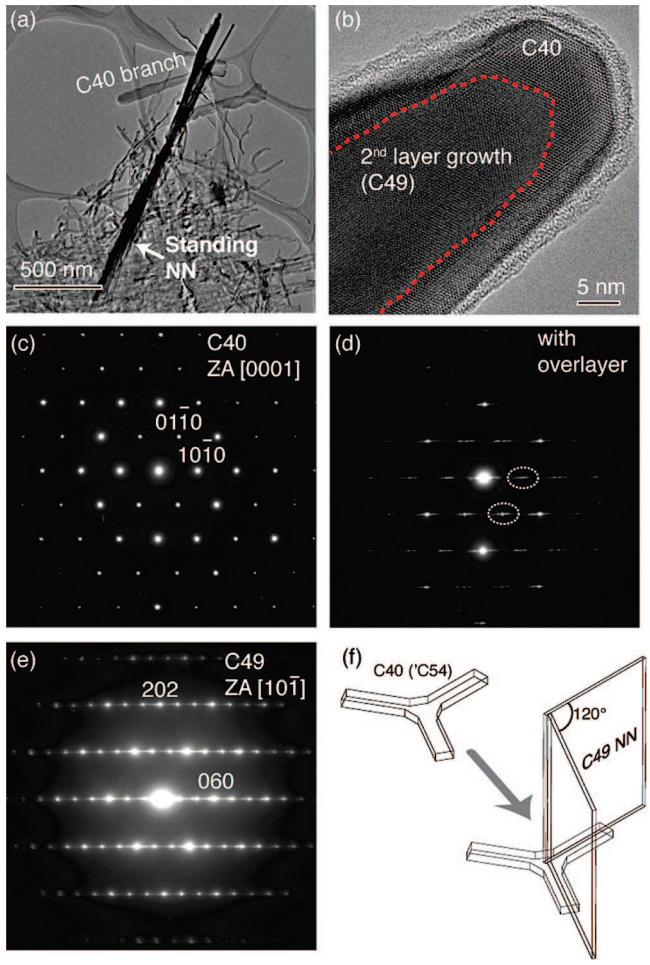

Figure 6. Growth mechanism of 3D $TiSi_2$ nanostructures. (a) TEM picture shows the existence of the C40 phase, branching out at the bottom of a C49 NN at 60°. (b) HRTEM picture reveals the growth of C49 $TiSi_2$ on top of {0001} planes of the C40 phase. (c−e) ED patterns of the C40 branch (c), with C49 deposition (d) and the C49 NN (e). The proposed growth model is schematically depicted in f.

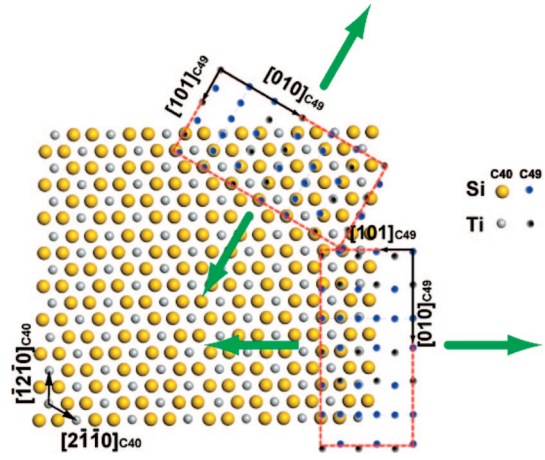

Figure 7. Atomic arranges of C40 and C49 $TiSi_2$. The possible overlap of them is shown in the rectangles. Green arrows indicate the growth direction of the C49 NNs as viewed from the top ([0001] direction of the C40 phase).

6d. The stretching features in the ED pattern unambiguously confirm the over layer growth. For a comparison, the ED pattern of the pure C49, which was taken from the standing NN, was presented in Figure 6e.

On the basis of this observation, we propose the growth mechanism as follows. Under the transitional conditions that both C54 and C49 $TiSi_2$ nanostructures cogrow, metastable C40 $TiSi_2$ emerges. It results in hexagonal branches like that shown in Figure 6f. However, the condition favors C49 NNs that will originate from the {0001} planes of C40. C54 NWs of $TiSi_2$ probably also grow equally well from the C40 branches. Without any unique patterns generated from such potential growth, its presence would be difficult to observe and confirm. On the other hand, the 2D nature of C49 $TiSi_2$ NNs presents a great opportunity to observe the existence of the metastable phases. The detailed atomic arrangements of the C40 branches and C49 NNs also support this proposed growth model. As shown in Figure 7, C49 $TiSi_2$ overlaps with C40 $TiSi_2$ with reasonable match. The growth directions of the NNs are perpendicular to [010], indicated by the green arrows, and develop to intersect each other at 120° angles. Additional growths of C49 NNs are likely to originate from the underlying C40 branches, yielding NNs parallel to the first grown ones. The fact that XRD data do not show corresponding peaks of C40 $TiSi_2$ may be because of the small amount.

Finally, it is noteworthy that we believe the growth of $TiSi_2$ nanostructures is not epitaxial as they appear to be insensitive to the collecting substrates. Substrates that survive the growth temperature, such as quartz, Ti foil, stainless steel plates and Si/SiO_2 were tested and comparable yield was achieved. These observations further support the spontaneous nucleation and growth model. We suggest that the initial nuclei are formed in the gas phase. Once formed, they are attracted to the receiving substrate by either gravity or van der Waals force. Si and Ti feedstocks from the gaseous reactions are added to the nuclei on the substrate and the growth continues.

In summary, $TiSi_2$ nanostructures with varying complexities were successfully synthesized through rational controls. The results were enabled by the understanding of the growth mechanisms. The crystal structures and surface atomic arrangements were found to play a key role in different morphology formations. These results are expected to shed light on rational nanostructure syntheses in general and eventually pave the way to the grand challenge of nanomaterials by design.

Acknowledgment. The work was supported by Boston College. The authors are grateful to Dr. D. Wang for his assistance with structural analysis. We also thank the reviewers for their constructive suggestions in revising this article.

Supporting Information Available: Experimental details of substrate cleaning; methodology of quantifying growth products (NNs vs NWs); comparison of lattice constants obtained in this work with literature; analysis of C54 surface energies; HRTEM of C54 and C49 $TiSi_2$; magnified view of Figure 1f in the main text; and schematic illustrations of $TiSi_2$ atomic arrangements (PDF). This material is available free of charge via the Internet at http://pubs.acs.org.

CM8023296